Article

Exceptional Framework Flexibility and Sorption Behavior of a Multifunctional Porous Cuprous Triazolate Framework

Jie-Peng Zhang, and Xiao-Ming Chen

J. Am. Chem. Soc., **2008**, 130 (18), 6010-6017 • DOI: 10.1021/ja800550a • Publication Date (Web): 03 April 2008

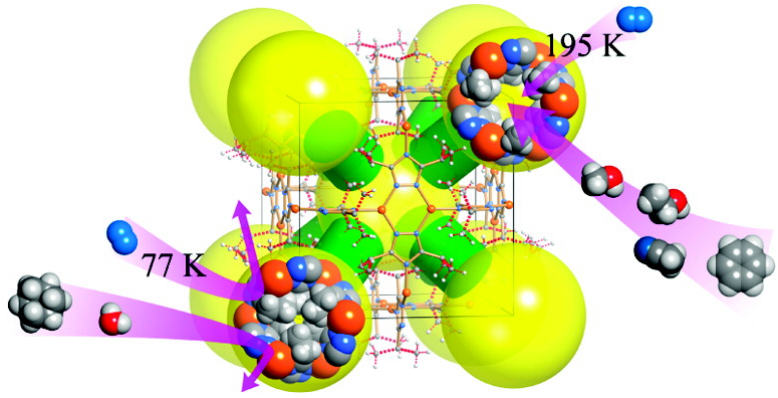

More About This Article

Additional resources and features associated with this article are available within the HTML version:

- Supporting Information
- Links to the 8 articles that cite this article, as of the time of this article download
- Access to high resolution figures
- Links to articles and content related to this article
- Copyright permission to reproduce figures and/or text from this article

View the Full Text HTML

J|A|C|S
ARTICLES

Published on Web 04/03/2008

Exceptional Framework Flexibility and Sorption Behavior of a Multifunctional Porous Cuprous Triazolate Framework

Jie-Peng Zhang* and Xiao-Ming Chen*

MOE Laboratory of Bioinorganic and Synthetic Chemistry, School of Chemistry and Chemical Engineering, Sun Yat-Sen University, Guangzhou 510275, China

Received January 23, 2008; E-mail: zhangjp7@mail.sysu.edu.cn (J.-P. Zhang); cxm@mail.sysu.edu.cn (X.-M. Chen)

Abstract: The porous metal azolate framework $[Cu(etz)]_\infty$ (MAF-2, Hetz = 3,5-diethyl-1,2,4-triazole) processes an NbO type cuprous triazolate scaffold and a CsCl type hydrophobic channel system, in which the large cavities are interconnected by small apertures with pendant ethyl groups. Since the ethyl-blocked apertures behave as thermoactivated IRIS stops for the guest molecules, the gas sorption behavior of MAF-2 can be controlled by temperature, in which N_2 adsorption was observed at 195 K rather than 77 K. Single-crystal X-ray structural analysis revealed that the $[Cu(etz)]_\infty$ host framework is not altered upon N_2 inclusion, confirming the occurrence of the so-called "*kinetically controlled flexibility*". By virtue of the kinetically controlled flexibility and hydrophobic pore surface, MAF-2 can adsorb large amounts of small organic molecules but excludes H_2O. As demonstrated by single-crystal X-ray structural analyses, MAF-2 shrinks, expands, or distorts its framework to accommodate the hydrogen-bonded hexamers of MeOH, EtOH, or MeCN, respectively. Moreover, MAF-2 can also separate benzene and cyclohexane efficiently, as its flexible scaffold can distort to a certain degree so that benzene can diffuse through the distorted apertures but cyclohexane cannot. Moreover, the adsorption/desorption of these organic vapors induces reversible, multimode structural transformations.

Introduction

The construction and characterization of porous coordination polymers (PCPs) with useful functionalities have been the focus of intense research activity. To achieve permanent porosity and high gas storage capacity, highly robust metal−organic frameworks have been the major research goal during the past decade.[1] Recently, the advantages of dynamic frameworks for high performance molecular recognition, separation, and sensing have attracted more and more attention.[2–6] Nevertheless, a given flexible framework usually adopts a single deformation mode such as expansion, contraction, or distortion upon guest inclusion. Obviously, a flexible PCP with a multimode structural transformation ability is more attractive as a multipurpose guest sensor and actuator.

Thermodynamic (structural) multistability is regarded as a sign of framework flexibility, and most attention has been focused on the guest-induced structural transformations at equilibrium states.[2–6] However, some flexible frameworks may temporarily open their small apertures to allow the diffusion of oversize guest species and keep the host structure unchanged after guest inclusion.[7–10] The combination of structural flexibility and thermodynamic monostability arises from the transient structural transformation to the thermodynamically and kinetically unstable state. In the energy diagram (Scheme 1), a rigid framework is associated with a single energy minimum, but a flexible framework has two (or more) local energy minima. Usually, the local energy minima are well separated by energy barriers much higher than the thermal vibration energy ($E_a >>$

Scheme 1. Energy Diagrams of the Rigid and Flexible Frameworks

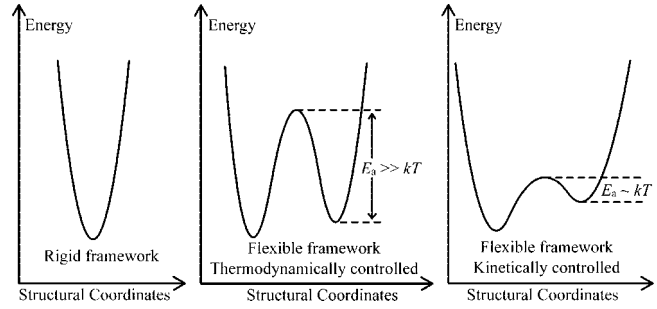

(1) Yaghi, O. M.; O'Keeffe, M.; Ockwig, N. W.; Chae, H. K.; Eddaoudi, M.; Kim, J. *Nature* **2003**, *423*, 705–714.
(2) (a) Kitagawa, S.; Kitaura, R.; Noro, S. I. *Angew. Chem., Int. Ed.* **2004**, *43*, 2334–2375. (b) Kitagawa, S.; Uemura, K. *Chem. Soc. Rev.* **2005**, *34*, 109–119.
(3) Bradshaw, D.; Claridge, J. B.; Cussen, E. J.; Prior, T. J.; Rosseinsky, M. J. *Acc. Chem. Res.* **2005**, *38*, 273–282.
(4) Kepert, C. J. *Chem. Commun.* **2006**, 695–700.
(5) Férey, G. *Chem. Soc. Rev.* **2008**, *37*, 191–214.
(6) (a) Halder, G. J.; Kepert, C. J. *Aust. J. Chem.* **2006**, *59*, 597–604. (b) Suh, M. P.; Cheon, Y. E. *Aust. J. Chem.* **2006**, *59*, 605–612. (c) Kawano, M.; Fujita, M. *Coord. Chem. Rev.* **2007**, *251*, 2592–2606.
(7) (a) Barbour, L. J. *Chem. Commun.* **2006**, 1163–1168. (b) Dalgarno, S. J.; Thallapally, P. K.; Barbour, L. J.; Atwood, J. L. *Chem. Soc. Rev.* **2007**, *36*, 236–245.
(8) Cussen, E. J.; Claridge, J. B.; Rosseinsky, M. J.; Kepert, C. J. J. *Am. Chem. Soc.* **2002**, *124*, 9574–9581.
(9) (a) Zhao, X.; Xiao, B.; Fletcher, A. J.; Thomas, K. M.; Bradshaw, D.; Rosseinsky, M. J. *Science* **2004**, *306*, 1012–1015. (b) Liu, Y.; Eubank, J. F.; Cairns, A. J.; Eckert, J.; Kravtsov, V. C.; Luebke, R.; Eddaoudi, M. *Angew. Chem., Int. Ed.* **2007**, *46*, 3278–3283. (c) Pan, L.; Olson, D.-H.; Ciemnolonski, L. R.; Heddy, R.; Li, J. *Angew. Chem., Int. Ed.* **2006**, *45*, 616–619.
(10) Takamizawa, S.; Kohbara, M.-A. *Dalton. Trans.* **2007**, *42*, 3640–3645.

10.1021/ja800550a CCC: $40.75

kT), so the structural flexibility is dominated by thermodynamic multistability, and structural interconversion is controlled by thermodynamic factors such as adsorption/desorption of guest molecules. When energy barriers are comparable to, or smaller than, the thermal vibration energy ($E_a \approx kT$), the higher local energy minima become unstable and quickly relax to the single thermodynamically and kinetically stable state. Consequently, no thermodynamic multistability is present, and structural flexibility/interconversion is now dominated by kinetic factors such as the diffusion of guest molecules. Therefore, this unique structural flexibility can be denoted as *kinetically controlled flexibility* (KCF), in contrast with the *thermodynamically controlled flexibility* (TCF) arisen from the thermodynamic multistability. The low energy barrier nature of this system implies that the framework flexibility can be easily tuned by external variables,[11] pointing to a novel family of porous materials whose porous properties can respond to physical stimuli such as an electric field and heat.[12]

The KCF of a dynamic framework is suggested by the smaller size of the channel apertures compared with the molecular dimensions of the guests and corroborated by the negligible framework alteration after guest inclusion. Unfortunately, unambiguous KCF is difficult to be confirmed due to the lack of sufficient structural information of the guest-free and guest-included materials[7–10,12] or the coexistence of KCF and TCF.[13,14] KCF can arise from several dynamic mechanisms such as framework distortion, internetwork (intermolecular) displacement, and other molecular motions that dispense with the framework distortion or internetwork displacement. Framework distortion and internetwork displacement can produce large structural and energetic differences, which is a key feature for dynamic behaviors such as diffusion of oversize guests and abnormal sorption isotherms. However, these large differences imply that the host framework can easily undergo permanent structural transformation upon sorption, leading to TCF rather than KCF. Either permanent or momentary, these mechanisms induce lattice distortions and stresses that tend to fracture the large single crystals, making direct/precise structural characterization difficult.[6,15,16] On the other hand, some molecular motions, such as the rotation/swing of noncoordinated functional groups in PCPs, may dispense with framework distortion or internetwork displacement,[17–19] avoiding the above-mentioned disadvantages. Nevertheless, such dynamic motions usually generate relatively small aperture variations[7,12] and/or disordered structures.[17–19] Therefore, rational design and a conclusive demonstration of a KCF dominated dynamic porous framework remain an ongoing challenge.

Metal azolate frameworks (MAFs) have attracted much attention in the aspects of crystal engineering in recent years.[14,19–21] We have designed and synthesized a NbO-type[22] cuprous triazolate framework $\{[Cu(etz)]\cdot guest\}_\infty$ (Hetz = 3,5-diethyl-1,2,4-triazole) with cubic symmetry (MAF-2c·g) by the aid of a solvothermal in situ ligand/metal reaction of cupric salt, propionitrile, and ammonia.[19] MAF-2c possesses a 3D intersecting pore system whose large cavities are interconnected via short, small channels. Interestingly, the apertures of these channels are blocked by pendant, disordered ethyl groups with rotation/swing flexibility and may be continuously tuned from closed to open by cooperative motions of the ethyl groups without disrupting the $[Cu(tz)]_\infty$ (tz = triazolato ring) scaffold, being similar to the IRIS stop used in optical cameras (Figure 1). Nevertheless, besides the symmetry-imposed disorder,[10,18] MAF-2c·g loses guest molecules and single crystallinity to form a new material with an unknown structure,[19] precluding further verification of its KCF.

We report herein the direct synthesis, structure, and property of this new material. Guest-free $[Cu(etz)]_\infty$ was obtained as a trigonal phase (MAF-2) without any symmetry-imposed disorder. This material demonstrated exceptional framework flexibility and sorption properties, e.g., temperature-controllable sorption behavior, superior organic solvent/water and benzene/cyclohexane selectivity, and multimode structural transformations.

Experimental Section

Materials and Physical Measurements. Commercially available reagents were used as received without further purification. Hetz was synthesized by a reported method.[23] Elemental analyses (C, H, N) were performed on a Perkin-Elmer 240 elemental analyzer. Thermal gravimetric analysis was performed under N_2 using a NETZSCH TG 209 system. Powder X-ray diffraction patterns were measured at a Rigaku D/M-2200T automated diffractometer. Gas and solvent vapor sorption isotherms were measured on a volumetric adsorption apparatus (Bel-max).

Synthesis of $[Cu(etz)]_\infty$ (MAF-2). A solution of Hetz (4.0 mmol) in methanol (100 mL) was dropwise added into a solution of $[Cu(NH_3)_2]OH$ (4.0 mmol) in aqueous ammonia/methanol (1/1, 100 mL) with stirring at room temperature under N_2 atmosphere. The mixture was aged at 50 °C for 3 h and then evacuated under vacuum until half of the solvent was recovered. The white crystalline powder was filtered, washed with methanol, and dried in vacuum to give MAF-2 (yield 80–100% depending on the solvent recovery ratio). Anal. Calcd (%) for $C_6H_{10}CuN_3$: C, 38.39; H, 5.37; N, 22.39. Found: C, 38.35; H, 5.43; N, 22.48. Large single crystals of MAF-2

(11) (a) Wu, C.-D.; Hu, A.; Zhang, L.; Lin, W.-B. *J. Am. Chem. Soc.* **2005**, *127*, 8940–8941. (b) Llewellyn, P. L.; Bourrelly, S.; Serre, C.; Filinchuk, Y.; Férey, G. *Angew. Chem., Int. Ed.* **2006**, *45*, 7751–7754. (c) Maji, T. K.; Matsuda, R.; Kitagawa, S. *Nat. Mat.* **2007**, *6*, 142–148. (d) Dincă, M.; Long, J. R. *J. Am. Chem. Soc.* **2007**, *129*, 11172–11176. (e) Mulfort, K. L.; Hupp, J. T. *J. Am. Chem. Soc.* **2007**, *129*, 9604–9605. (f) Kawano, M.; Kawamichi, T.; Haneda, T.; Kojima, T.; Fujita, M. *J. Am. Chem. Soc.* **2007**, *129*, 15418–15419.
(12) (a) Chen, B.-L.; Ma, S.-Q.; Zapata, F.; Fronczek, F. R.; Lobkovsky, E. B.; Zhou, H.-C. *Inorg. Chem.* **2007**, *46*, 1233–1236. (b) Ma, S.-Q.; Sun, D.-F.; Wang, X.-S.; Zhou, H.-C. *Angew. Chem., Int. Ed.* **2007**, *46*, 2458–2462.
(13) Atwood, J. L.; Barbour, L. J.; Jerga, A.; Schottel, B. L. *Science* **2002**, *298*, 1000–1002.
(14) Zhang, J.-P.; Kitagawa, S. *J. Am. Chem. Soc.* **2008**, *130*, 907–917.
(15) Rather, B.; Zaworotko, M. J. *Chem. Commun.* **2003**, 830–831.
(16) Vittal, J. J. *Coord. Chem. Rev.* **2007**, *251*, 1781–1795.
(17) Horike, S.; Matsuda, R.; Tanaka, D.; Matsubara, S.; Mizuno, M.; Endo, K.; Kitagawa, S. *Angew. Chem., Int. Ed.* **2006**, *45*, 7226–7230.
(18) Eddaoudi, M.; Kim, J.; Rosi, N.; Vodak, D.; Wachter, J.; O'Keeffe, M.; Yaghi, O. M. *Science* **2002**, *295*, 469–472.
(19) Zhang, J.-P.; Huang, X.-C.; Lin, Y.-Y.; Chen, X.-M. *J. Am. Chem. Soc.* **2005**, *127*, 5495–5506.
(20) (a) Masciocchi, N.; Galli, S.; Sironi, A. *Comments Inorg. Chem.* **2005**, *26*, 1–37. (b) Zhang, J.-P.; Chen, X.-M. *Chem. Commun.* **2006**, 1689–1699.
(21) (a) Huang, X.-C.; Lin, Y.-Y.; Zhang, J.-P.; Chen, X.-M. *Angew. Chem., Int. Ed.* **2006**, *45*, 1557–1559. (b) Park, K. S.; Ni, Z.; Côté, A. P.; Choi, J. Y.; Huang, R.; Uribe-Romo, F. J.; Chae, H. K.; O'Keeffe, M.; Yaghi, O. M. *Proc. Natl. Acad. Sci. U.S.A.* **2006**, *103*, 10186–10191. (c) Tian, Y.-Q.; Zhao, Y.-M.; Chen, Z.-X.; Zhang, G.-N.; Weng, L.-H.; Zhao, D.-Y. *Chem.—Eur. J.* **2007**, *13*, 4146–4154. (d) Hayashi, H.; Côté, A. P.; Furukawa, H.; O'Keeffe, M.; Yaghi, O. M. *Nat. Mater.* **2007**, *6*, 501–506.
(22) (a) Chen, B.-L.; Ockwig, N. W.; Millward, A. R.; Contreras, D. S.; Yaghi, O. M. *Angew. Chem., Int. Ed.* **2005**, *44*, 4745–4749. (b) Lin, X.; Jia, J.-H.; Zhao, X.-B.; Thomas, K. M.; Blake, A. J.; Walker, G. S.; Champness, N. R.; George, M. W.; Hubberstey, P.; Schröder, M. *Angew. Chem., Int. Ed.* **2006**, *45*, 7358–7364.
(23) van Albada, G. A.; de Graaff, R. A. G.; Haasnoot, J. G.; Reedijk, J. *Inorg. Chem.* **1984**, *23*, 1404–1408.

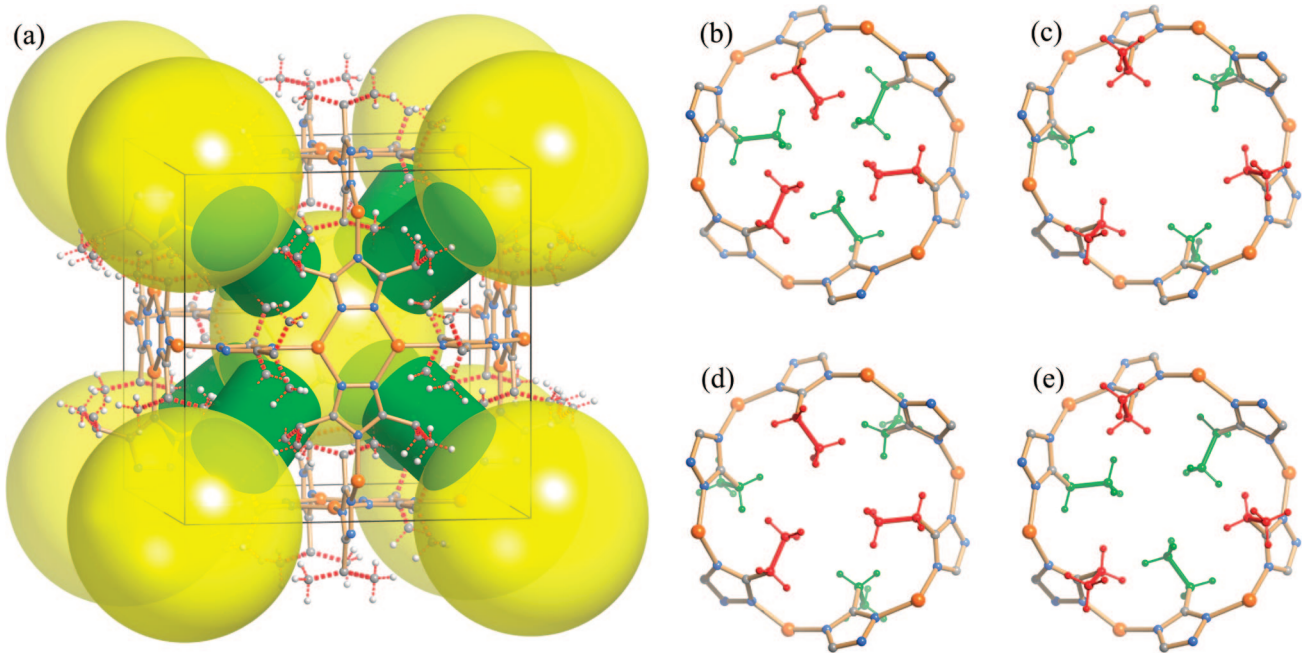

Figure 1. (a) NbO type coordination framework (2-fold disordered ethyl groups are shown as dashed bonds in red) and bcu type pore network (large yellow sphere: large pore inside the NbO cage; green column: short channel with double gate) structures of $[Cu(etz)]_\infty$. Each gate can tune its aperture size independently by rotation/swing motions of the three pendant ethyl groups without disrupting the $[Cu(tz)]_\infty$ scaffold. (b−e) Perspective views of four representative channel states derived from the crystal structure of MAF-2c, i.e., double closed, double open, closed-open, and open-closed, respectively (ethyl groups are colored in red and green to highlight the two different gates). Note that all channels can simultaneously adopt the closed-open/open-closed state, giving rise to a nonpermeable structure in the static point of view.

Table 1. Crystallographic Data and Refinement Parameters[a]

	MAF-2c · g[19]	MAF-2	MAF-2 · N_2	MAF-2 · MeOH	MAF-2 · EtOH	MAF-2t · MeCN
formula	$C_6H_{12}CuN_3O$	$C_6H_{10}CuN_3$	$C_6H_{10}CuN_4$	$C_7H_{14}CuN_3O$	$C_8H_{16}CuN_3O$	$C_{24}H_{39}Cu_3N_{12}$
FW	205.73	187.71	201.72	219.75	233.78	686.29
space group	$Im\bar{3}$	$R\bar{3}$	$R\bar{3}$	$R\bar{3}$	$R\bar{3}$	$P\bar{1}$
T/K	123(2)	123(2)	93(2)	123(2)	123(2)	123(2)
a/ Å	14.9159(7)	19.6891(8)	19.6052(5)	19.429(2)	19.810(3)	11.949(2)
b/ Å	14.9159(7)	19.6891(8)	19.6052(5)	19.429(2)	19.810(3)	12.263(4)
c/ Å	14.9159(7)	14.1971(7)	14.2420(4)	14.321(2)	14.180(2)	13.213(4)
α/deg	90	90	90	90	90	108.677(2)
β/deg	90	90	90	90	90	108.348(1)
γ/deg	90	120	120	120	120	104.458(3)
V/Å^3	3318.6(3)	4766.3(4)	4740.7(2)	4681.7(8)	4819.2(12)	1603.2(7)
Z	12	18	18	18	18	2
D_c/g cm^{-3}	1.236	1.177	1.272	1.403	1.450	1.422
μ/mm^{-1}	1.934	2.007	2.025	2.061	2.007	2.005
R_1 ($I > 2\sigma$)	0.0531	0.0402	0.0327	0.0266	0.0363	0.0436
wR_2 (all data)	0.1572	0.0770	0.0761	0.0587	0.0993	0.0887
GOF	1.082	1.014	1.015	1.037	1.031	1.010
void/%	39.7	33.4	32.7	32.2	35.4	37.3

[a] $R_1 = \Sigma F_o| - |F_c/\Sigma|F_o|$, $wR_2 = [\Sigma w(F_o^2 - F_c^2)^2/\Sigma w(F_o^2)^2]^{1/2}$.

were obtained by heating the mixture in a Teflon-lined autoclave at 120 °C for 2 days, followed by filtration and drying in vacuum.

X-Ray Crystallography. The solvent-loaded single crystals were prepared by exposing MAF-2 in the corresponding solvent vapor for a few days. Diffraction intensities were collected on a Bruker Apex CCD area-detector diffractometer (Mo Kα). The structures were solved with direct methods and refined with a full-matrix least-squares technique with the SHELXTL program package.[24] Dinitrogen molecules were refined as a 2-fold disorder with a 0.25 + 0.25 occupancy and a N−N distance of 1.10(1) Å. Anisotropic thermal parameters were applied to all non-hydrogen atoms except the disordered EtOH molecules. The organic hydrogen atoms were generated geometrically. Solvent accessible volumes (void/%) for the $[Cu(etz)]_\infty$ frameworks were calculated by the SOLV routine of PLATON 2003.[25] Crystal data and refinement parameters for the complexes are summarized in Table 1.

Results and Discussion

Material Synthesis. The cubic phase MAF-2c·g was originally synthesized in low yield (10–15%) by a solvothermal in situ metal/ligand reaction of cupric salt, propionitrile, and ammonia.[19] Due to the symmetry-imposed disorder of the ethyl groups, it is difficult to make a conclusive structural interpretation of the ethyl conformations around each aperture. Moreover, MAF-2c·g easily loses guest molecules and single-crystallinity,

(24) *SHELXTL 6.10*; Bruker Analytical Instrumentation: Madison, Wisconsin, USA, 2000.

(25) Spek, A. L. *PLATON*, Utrecht University: Utrecht, The Netherlands, 2003.

transforming into a guest-free crystalline phase (MAF-2) with an unknown structure.

The preparative difficulty is commonly encountered in the production of coordination polymers. Actually, the simple chemical compositions of binary metal−azolate frameworks imply that these materials can be facilely synthesized by simple acid–base reactions. Simply mixing $[Cu(NH_3)_2]OH$ and Hetz in aqueous ammonia/methanol produces white crystalline powders. After removal of the solvent, the binary cuprous triazolate can be isolated in quantitative yield. According to the elemental analysis and PXRD patterns, the product displays a composition and diffraction pattern identical to those of the guest-free MAF-2. Large, high-quality single crystals of MAF-2 can be obtained by a solvothermal treatment of the reaction mixture.

Framework Structure. The cubic MAF-2c possesses a regular ($Im\bar{3}$) NbO-type $[Cu(tz)]_\infty$ scaffold, which is constructed by interconnection of square-planar nodes ($\{Cu_2(tz)_2\}$ fragments) with a 90° interplanar angle between adjacent $\{Cu_2(tz)_2\}$ fragments. The structural information of the 3D NbO network can be simply visualized from its cagelike fragments (NbO cages). The large cavities (d = 9 Å) inside the NbO cages interconnect via eight hexagonal $\{Cu_6(etz)_6\}$ rings (chair conformation) to form a 3D intersecting pore system (void = 39.7%) with a regular bcu topology (dual net of NbO).[26] The chairlike, hexagonal $\{Cu_6(etz)_6\}$ ring defines a short channel with a double gate. From the static point of view, all channels of MAF-2c appear to be simultaneously closed (d = 1.5 Å, smaller than any real molecule) by the pendant ethyl groups. Considering the rotation/swing flexibility of ethyl groups, the apertures may be continuously tuned to the open state, which permits the passage of a sphere with d < 3.6 Å or an irregular particle with the smallest cross-sectional dimensions <4.2 Å (such as methane and nonbranched hydrocarbons). The suitable aperture-size variation implies that MAF-2c may potentially show KCF for a variety of guest molecules (Figure 1). Nevertheless, symmetry-imposed disorder of the ethyl groups precludes any conclusive interpretation based on the crystal structure of MAF-2c.

Single-crystal X-ray diffraction analysis of MAF-2 revealed one Cu(I) cation and one etz anion in the crystallographically asymmetric unit and a distorted NbO type $[Cu(etz)]_\infty$ network, without any symmetry-imposed disorder ($R\bar{3}$). As the local coordination geometries of MAF-2c and MAF-2 are very similar, the network distortion should mainly arise from the rotation between adjacent $\{Cu_2(tz)_2\}$ moieties, which reduces the interplanar angles from 90° to 79°. Straightforwardly, the unit-cell parameters of MAF-2 (a, 19.6891 Å; c, 14.1971 Å; and V, 4766.3 Å^3) are significantly different from the trigonal setting ones of MAF-2c (a, 21.0943 Å; c, 12.9175 Å; and V, 4977.8 Å^3). The transformation from MAF-2c to MAF-2 includes a large expansion in the c-axis (9.9%) and a large contraction in the ab plane (6.7% in axis length, 12.9% in area), resulting in an anisotropic contraction (4.2% in volume). The NbO cages and cavities also distort in the same manner. The eight equivalent $\{Cu_6(etz)_6\}$ rings of MAF-2c disproportion into two types in MAF-2. The first type consists of two $\{Cu_6(etz)_6\}$ rings (running along the c-axis), which are identical to the double-closed channels of MAF-2c. The other six $\{Cu_6(etz)_6\}$ rings form the second type of channels, which are distorted in the same manner as the lattice, but are completely blocked by only two ethyl groups (Figure 2). Consequently, the unoccupied space inside MAF-2 can be safely described as isolated cavities, from the static point of view. On the other hand, the momentary rotation/swing motion of the ethyl groups can allow the passage of small guest molecules (as large as nonbranched hydrocarbons), without disrupting the $[Cu(tz)]_\infty$ scaffold. Therefore, MAF-2 represents as a suitable candidate for the study of KCF.

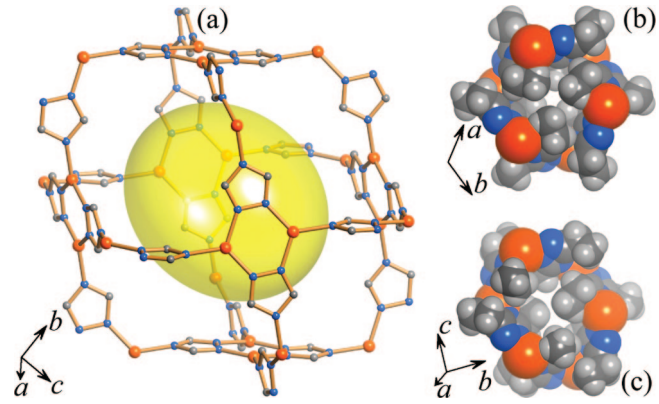

Figure 2. Perspective views of the distorted NbO type [Cu(tz)] scaffold (a) and the ethyl-blocked channels (b: running along the c-axis, c: running slanted to the c-axis) of MAF-2.

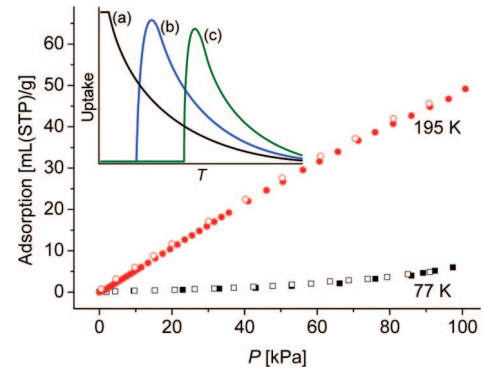

Figure 3. N_2 sorption isotherms of MAF-2. Inset: Characteristic adsorption isobars for rigid porous materials (a) and flexible porous materials with temperature-dependent aperture size (b: for small guest, c: for large guest).

Framework Stability. According to thermal gravimetric (TG) analysis and X-ray diffraction studies, the guest-free MAF-2 does not change its structure (except small thermal expansion that has negligible impact on the static aperture size) from cryogenic to high temperature until decomposition above ~280 °C. Although MAF-2 is constructed by three-coordinated (or coordinatively unsaturated) cuprous centers, its chemical stability is remarkable.[14] The microcrystalline powder sample of the guest-free MAF-2 can be handled in air, and its color changes from white to light green after several weeks depending on the humidity, implying the oxidation of Cu(I) in air is promoted by moisture. However, after prolonged exposure, the PXRD pattern of the light-green product still resembles that of MAF-2 (except some peak weakening), implying that the oxidation occurred on the particle surface rather than the pore surface. The hydrophobic, isolated pore system of MAF-2 is responsible for these observations, as the water molecules may hardly pass through the hydrophobic, closed channels.

Gas Sorption. Dinitrogen sorption isotherms for MAF-2 were measured at 77 and 195 K (Figure 3). Consistent with its nonpermeable crystal structure, MAF-2 completely excludes N_2

(26) Friedrichs, O. D.; O'Keeffe, M.; Yaghi, O. M. *Acta Crystallogr., Sect. A* **2003**, *59*, 22–27.

at 77 K. On the other hand, MAF-2 can readily adsorb supercritical N_2 at 195 K. The adsorption amount at 1 atm (49 mL/g) corresponds to 0.41 N_2 per formula unit or 2.5 N_2 per NbO cage, indicating the N_2 molecules are adsorbed into the cavities of MAF-2 rather than the particle surface. Because the static aperture size of MAF-2 is too small for any real molecule, the apertures must open during the sorption process. The abnormal temperature-dependent sorption behavior of MAF-2 is in contrast with those of rigid porous frameworks. When the temperature increases, the adsorption capacity of a rigid porous material at a given guest pressure decreases monotonously because the saturation pressure of the guest increases and the host–guest interaction decreases. However, flexible frameworks may start to adsorb a given gas until the temperature is high enough to open their apertures to allow the diffusion of the guest molecules. In contrast to the monotonously decreasing isobar of a rigid porous material, there is a characteristic onset adsorption (gate opening) temperature in the isobar of such a flexible material. In the case of MAF-2, the temperature-dependent gate-opening behavior should arise from the ethyl-blocked apertures, which behave as thermoactivated IRIS stops. As the effective aperture sizes of these flexible materials vary with temperature, size-different guest molecules could have different onset adsorption temperatures. Obviously, these flexible materials are of great importance in multipurpose gas separation.[12]

It should be noted that, the temperature-dependent gate-opening behavior could be derived from not only KCF, but also temperature-driven structure variation of the guest-free host framework. Nevertheless, the temperature-driven structure variation of the guest-free MAF-2 has been ruled out by single-crystal and powder X-ray diffraction studies. We also determined the structure of the gas-loaded single crystal to confirm that thermodynamic bistability is not involved in the gas sorption process of MAF-2. Direct structural information of the absorbed gas molecules is fundamental to the understanding of adsorption mechanism and rational design of porous frameworks. Due to the extremely weak host–guest interaction, crystal structure determination of the gas-loaded phases remains a great challenge. Although some successes have been achieved for the gas-loaded PCPs with very small pores (strong confinement for the gas),[27–29] crystal structures concerning gas molecules absorbed in large pores are still very scarce.[30] In our experiment, a fully degassed single crystal of MAF-2 was filled with N_2 and flame-sealed in a glass capillary and then the temperature was decreased very slowly to 93 K in a cold dinitrogen flow, ensuring as much N_2 as possible is adsorbed at high temperature but the diffraction data were collected at low temperature (Table 1). Except some negligible thermal contraction, the host framework of the N_2-loaded MAF-2 is identical to that of the guest-free one, precluding the occurrence of thermodynamic bistability during the adsorption process. Therefore, the gas sorption mechanism of MAF-2 can be safely assigned to the KCF originated from the momentary rotation/swing motions of the ethyl groups. Interestingly, although the large cavity of

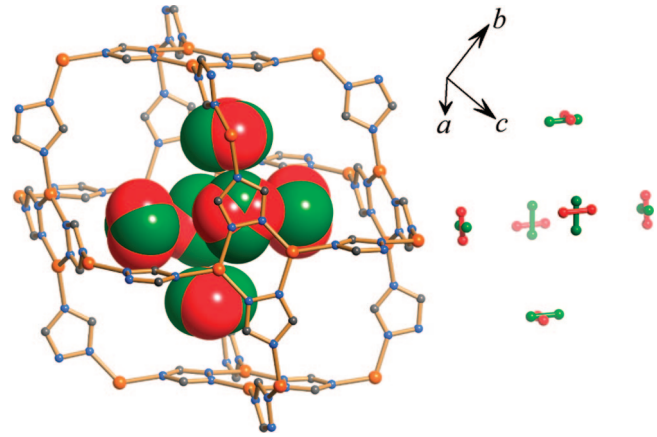

Figure 4. Perspective views of the absorbed N_2 molecules (2-fold disordered sites are represented in red and green) in space-filling (left, with an NbO cage) and ball-and-stick modes (right).

MAF-2 is not expected to strongly confine the partially loaded N_2 molecules at 93 K, the N_2 molecules were nicely refined in a 2-fold disordered model. The N_2 molecules form close contacts to the triazolato rings, and each N_2 is either parallel (N···N 3.33–3.41 Å) or staggered (N···N 3.52–3.54 Å) in relation to the 1,2-nitrogen atoms of etz (Figure 4). The intermolecular contacts between the N_2 molecules (shortest N···N 4.17 Å, center···center 4.79 Å) are substantially longer than other known values,[30] indicating relatively strong adsorbent–adsorbate interactions in MAF-2·N_2.

Vapor Sorption. Recovery, removal, and detection of small amounts of organic solvents from water, which rely on the selective binding of organic solvents over water, are of great technical, industrial, and environmental importance. Hydrophilic/hydrophobic affinity and pore size considerations are generally used to engineer porous materials with different binding abilities between water and organic solvents. Because hydrophilic building blocks are commonly used, many inorganic and metal−organic porous materials are known to adsorb water over organic molecules. Moreover, because the molecular size or kinetic diameter of H_2O is smaller than those of organic solvent molecules, size selective porous materials can only adsorb small water molecules over large organic molecules. Nevertheless, for PCPs, hydrophobic pore surfaces can be rationally introduced to adsorb organic molecules over H_2O. Li et al. have reported a hydrophobic PCP, zinc 5-*tert*-butyl isophthalate, which exhibits essentially zero water adsorption (~1 mg/g) up to the humidity $P/P_0 = 0.65$ but significant MeOH adsorption (110 mg/g at $P/P_0 = 0.73$).[31] Nevertheless, due to the large pore size required for the accommodation of organic molecules, capillary condensation of H_2O usually occurs for these hydrophobic porous materials at relatively high humidity and significantly reduces the organic/water selectivity. For example, Kitagawa et al. have demonstrated that a PCP with a hydrophobic pore surface does not show water uptake until $P/P_0 = 0.59$, which then abruptly rise to a high value (128 mg/g) at higher humidity.[32]

Inspired by the hydrophobic and closed channel structure, we anticipated that MAF-2 could selectively separate organic solvents from water. Water, methanol, ethanol, and acetonitrile

(27) (a) Matsuda, R.; Kitaura, R.; Kitagawa, S.; Kubota, Y.; Belosludov, R. V.; Kobayashi, T. C.; Sakamoto, H.; Chiba, T.; Takata, M.; Kawazoe, Y.; Mita, Y. *Nature* **2005**, *436*, 238–241.
(28) Kubota, Y.; Takata, M.; Kobayashi, T. C.; Kitagawa, S. *Coord. Chem. Rev.* **2007**, *251*, 2510–2521.
(29) Takamizawa, S.; Nakata, E.-I.; Akatsuka, T. *Angew. Chem., Int. Ed.* **2006**, *45*, 2216–2221.
(30) Rowsell, J. L. C.; Spencer, E. C.; Eckert, J.; Howard, J. A. K.; Yaghi, O. M. *Science* **2005**, *309*, 1350–1354.
(31) Pan, L.; Parker, B.; Huang, X.-Y.; Olson, D. L.; Lee, J. Y.; Li, J. *J. Am. Chem. Soc.* **2006**, *128*, 4180–4181.
(32) Horike, S.; Tanaka, D.; Nakagawa, K.; Kitagawa, S. *Chem. Commun.* **2007**, 3395–3397.

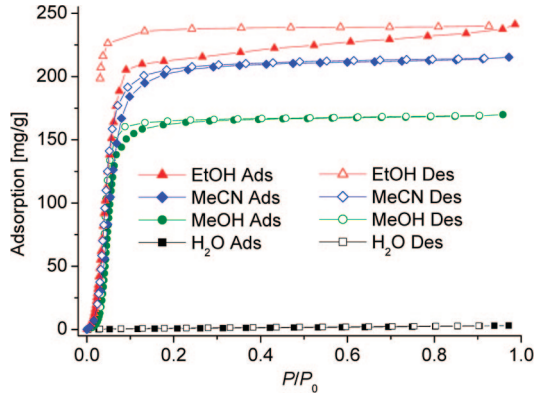

Figure 5. H_2O, MeOH, EtOH, and MeCN sorption isotherms measured at 298 K. P_0 is the saturation pressure (H_2O 3.17 kPa, MeOH 16.94 kPa, EtOH 7.87 kPa, MeCN 11.80 kPa).

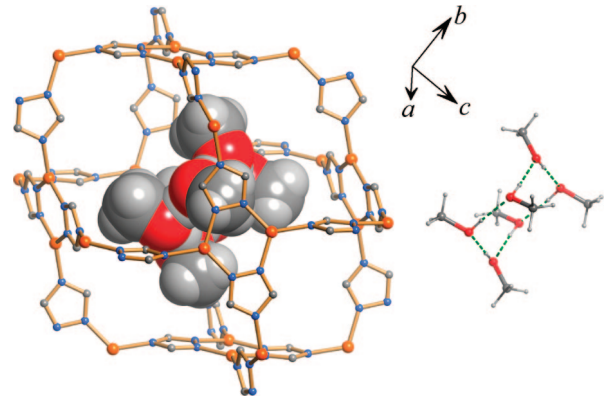

Figure 6. Perspective views of the MeOH hexamer in space-filling (left, with a NbO cage) and ball-and-stick modes (right).

vapor sorption isotherms for MAF-2 were measured at 298 K. As shown in Figure 5, MAF-2 exhibits a remarkable water resistance in the whole measured humidity range. The extremely low water uptake of MAF-2 (3 mg/g at $P/P_0 = 0.97$) can be attributed to particle surface adsorption on uncoordinated defects, indicating essentially no water molecules can diffuse through the ethyl-blocked channels into the NbO cages. On the other hand, MAF-2 can adsorb large amounts of MeOH, EtOH, and MeCN even at low relative pressures. The existence of onset adsorption pressures of these organic solvents near $P/P_0 = 0.02$ indicates that the adsorption processes are restricted by diffusion barriers and/or weak host–guest interactions below the critical points. Obviously, the diffusion barriers are related to the ethyl-blocked apertures. Nevertheless, these organic solvents can open the ethyl-blocked channels to access the large internal cavities, but water cannot. Therefore, organic solvent/water separation can be performed at very high humidity (i.e., small amounts of organic solvents vs large amount of water), which is close to the practical requirements. The weaker permeability of water compared to small organic solvents should be ascribed to the hydrophobicity of the ethyl groups, which interact very differently to water and organic molecules. This unique instance demonstrated a viable strategy for designing porous materials with high organic molecule/water selectivity, in which flexible, hydrophobic apertures are utilized to block the large internal cavities.

To elucidate the adsorption mechanism of MeOH, EtOH, and MeCN, we also measured the crystal structures of the solvent-loaded MAF-2. Interestingly, the single crystals of the guest-free MAF-2 have a high tendency to crack into smaller pieces in the MeCN vapor, while MeOH and EtOH vapors do not induce a significant change on the single crystal morphology. These phenomena are correlated to the degree of structural transformation upon solvent inclusion. The crystal structures of the MeOH- and EtOH-loaded materials are isostructural to the guest-free MAF-2, and the ethyl-blocked channels remain closed, confirming that KCF is dominant in the sorption processes of MeOH and EtOH. Nevertheless, small framework distortions are evident by comparing their unit-cell parameters. The inclusion of MeOH induces an anisotropic contraction (1.8% in volume), including a 1.3% contraction in the *a*-axis and a 0.9% expansion in the *c*-axis. In contrast, EtOH induces an anisotropic expansion (1.1% in volume), including a 0.6% expansion in the *a*-axis and a 0.1% contraction in the *c*-axis. Actually, the lattices of the guest-free and guest-loaded MAF-2 are different in the deviation degree from the cubic MAF-2c, in which the largest distortions (*ab* plane contraction, *c*-axis expansion, and volume contraction) are observed for MAF-2·MeOH, while MAF-2·EtOH adopts the smallest distortion. Inside the large NbO cage of MAF-2·MeOH, six MeOH molecules form a chairlike hydrogen-bonded (O···O 2.69 Å) hexagon with S_6 symmetry, and the hydrophobic methyl groups are exposed on the outer sphere with weak interactions to the triazolato rings (CH_3···N 3.66 Å) across the *ab* plane (Figure 6).[33] The framework contraction in the *ab* plane indicates that the MeOH hexamer is smaller than the NbO cage. More interestingly, the hydrogen-bonded MeOH hexamer behaves as a single molecule, which is relatively stiff to contract the flexible host framework rather than just expanding itself. The EtOH molecules also form similar hydrogen-bonded hexamers (disordered) in MAF-2·EtOH, but host framework must expand to accommodate the enlarged guest hexamers.

The adsorption of MeCN produces a triclinic structure, namely MAF-2t·MeCN, with highly unsymmetrical framework distortions, which can be evaluated by comparing its unit-cell parameters with the primitive unit-cell parameters of the cubic and trigonal phases (see Supporting Information). These distortions arise again from the rotations between adjacent $\{Cu_2(tz)_2\}$ fragments, as MAF-2t·MeCN still retains the original local coordination geometries and overall coordination topology. Moreover, some of the ethyl groups adopt new conformations, reflecting their rotation/swing flexibilities. MAF-2t possesses four (crystallographic) types of channels, which are all blocked by the ethyl groups. These structural features reveal that the adsorption mechanism involves not only TCF but also KCF. Interestingly, six MeCN molecules located inside the NbO cage of MAF-2t construct a trigonal prism cluster by weak C−H···N interactions (Figure 7). The shortest host–guest contacts are C−H···π (C···N 3.68 Å) and C−H···Cu (C···Cu 3.79 Å). To our knowledge, this is the first structurally characterized, matrix-isolated MeCN hexamer, which would be useful for the study of the structure and properties of acetonitrile.

The framework flexibility of MAF-2, as revealed from the diverse structural transformations, implies the hexagonal $\{Cu_6(tz)_6\}$ windows may undergo drastic distortions and cooperate with the KCF of ethyl groups to allow the passage of molecules which are larger than the above-studied guests, but other molecules exceeding the upper limit of these flexibilities will be excluded. Consequently, this hypothesis naturally

(33) Deiters, E.; Bulach, V.; Hosseini, M. W. *Chem. Commun.* **2005**, 3906–3908.

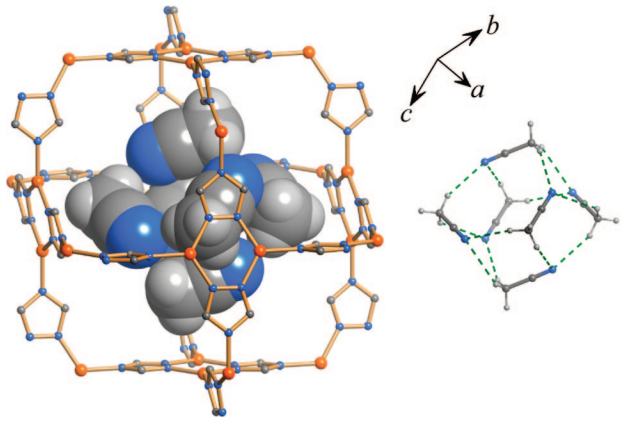

Figure 7. Perspective views of the MeCN hexamer in space-filling (left, with a NbO cage) and ball-and-stick modes (right).

points to a size-selective separation application, if we could find a pair of guest molecules with suitable sizes.[34] Distillation separation of benzene (C_6H_6) and cyclohexane (C_6H_{12}) is a highly demanded and energy-consuming process in the petrochemical industry, because C_6H_{12} is produced by hydrogenation of C_6H_6 in the C_6H_6/C_6H_{12} miscible system and the two substances have very similar boiling points (C_6H_6, 80.1 °C; C_6H_{12}, 80.7 °C). On the other hand, the chemical (C_6H_6, aromatic; C_6H_{12}, saturated) and molecular geometry (C_6H_6, 3.3 × 6.6 × 7.3 Å^3; C_6H_{12}, 5.0 × 6.6 × 7.2 Å^3)[35] differences between C_6H_6 and C_6H_{12} can be utilized for their effective separation.[36] The suitable and substantially different molecular sizes (smallest cross section) of C_6H_6 and C_6H_{12} could be used to test the framework flexibility upper limit of MAF-2. Indeed, MAF-2 can readily adsorb large amounts of C_6H_6 (206 mg/g or 3.0 C_6H_6 per NbO cage) but only exhibits particle surface adsorption for C_6H_{12} (9 mg/g at $P/P_0 = 0.96$, 0.1 C_6H_{12} per NbO cage). Although C_6H_6 is larger than MeOH, EtOH, and MeCN, its onset adsorption starts at a lower relative pressure ($P/P_0 = 0.01$), which may be ascribed to the stronger host–guest interactions arisen from the π system and C(sp^2)−H fragments (acidity stronger than that of C(sp^3)−H) of C_6H_6. The notable step in the isotherm near the uptake level of two C_6H_6 per NbO cage implies MAF-2 undergoes a significant structural transformation to accommodate one more C_6H_6 (Figure 8). We were not yet able to directly measure the crystal structure of the C_6H_6-loaded MAF-2, since the single crystals easily fracture into microcrystalline powders. However, these C_6H_6-loaded powders show the characteristic PXRD pattern of MAF-2c, whose framework structure is already known. Actually, the reversible organic vapor (MeOH, EtOH, MeCN, and C_6H_6) adsorption/desorption processes of MAF-2 can be conveniently monitored from their distinct PXRD patterns. Only very few PCPs have

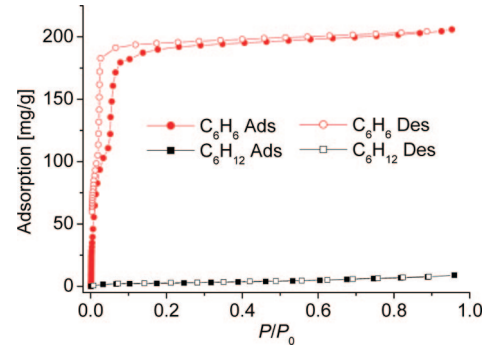

Figure 8. C_6H_6 and C_6H_{12} sorption isotherms measured at 298 K. P_0 is the saturation pressure (C_6H_6 12.69 kPa, C_6H_{12} 13.01 kPa).

Scheme 2. Vapor Responses of MAF-2[a]

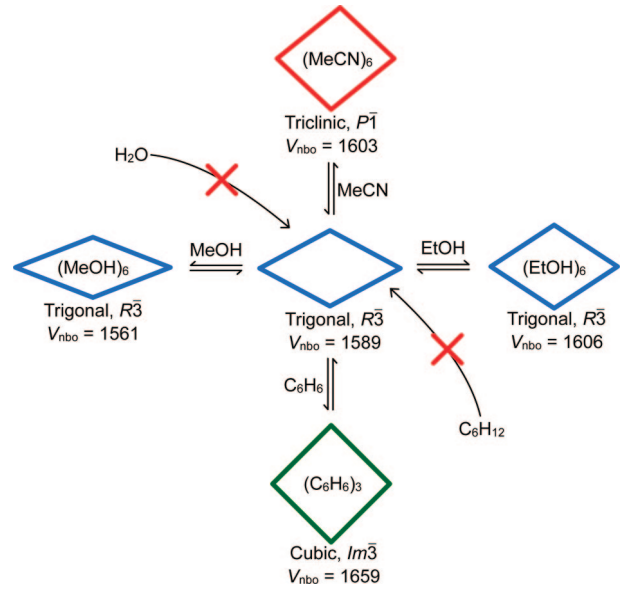

[a] V_{nbo} (Å^3) is the volume of one NbO cage fragment.

demonstrated a similar multimode structural transformation ability (Scheme 2).[37]

Conclusion

The novel structure of MAF-2 discovered in this work constitutes an excellent model for the study of KCF. According to the TG and X-ray diffraction studies of the guest-free and N_2-loaded MAF-2, the abnormal temperature-dependent sorption behavior of N_2 can be unambiguously assigned to KCF of MAF-2, in which the rotation/swing motions of the flexible ethyl groups are "frozen" below a critical or onset adsorption temperature. As the onset adsorption temperature depends on the size of the guest molecule, this type of PCP is potentially useful in the multipurpose gas separation.

By virtue of the KCF and hydrophobic channel apertures, MAF-2 exhibits superior organic solvent/water separation performance that is not likely accessible by traditional porous materials based on size and hydrophilicity/hydrophobicity-selective mechanisms. Although MAF-2 contains large cavities to adsorb guest molecules, H_2O cannot open the ethyl-blocked apertures, preventing the generally encountered capillary con-

(34) (a) Chen, B.-L.; Liang, C.-D.; Yang, J.; Contreras, D. S.; Clancy, Y.-L.; Lobkovsky, E. B.; Yaghi, O. M.; Dai, S. *Angew. Chem., Int. Ed.* **2006**, *45*, 1390–1393. (b) Alaerts, L.; Kirschhock, C. E. A.; Maes, M.; van der Veen, M. A.; Finsy, V.; Depla, A.; Martens, J. A.; Baron, G. V.; Jacobs, P. A.; Denayer, J. E. M.; de Vos, D. E. *Angew. Chem., Int. Ed.* **2007**, *46*, 4293–4297. (c) Yoon, J. W.; Jhung, S. H.; Hwang, Y. K.; Humphrey, S. M.; Wood, P. T.; Chang, J.-S. *Adv. Mater.* **2007**, *19*, 1830–1834.
(35) Webster, C. E.; Drago, R. S.; Zerner, M. C. *J. Am. Chem. Soc.* **1998**, *120*, 5509–5516.
(36) Shimomura, S.; Horike, S.; Matsuda, R.; Kitagawa, S. *J. Am. Chem. Soc.* **2007**, *129*, 10990–10991.
(37) (a) Dybtsev, D. N.; Chun, H.; Kim, K. *Angew. Chem., Int. Ed.* **2004**, *43*, 5033–5036. (b) Li, J.-Y.; Olson, D. H.; Pan, L.; Emge, T. J.; Li, J. *Adv. Funct. Mater.* **2007**, *17*, 1255–1262.

densation at high humidity. Consistent with the minor single-crystal structural variations, the sorption processes of MeOH and EtOH are also dominated by KCF.

In addition to the KCF of the pendant ethyl groups, the $[Cu(tz)]_\infty$ scaffold of MAF-2 also demonstrated an exceptional multimode structural transformation ability. MAF-2 not only expands to accommodate the oversize hydrogen-bonded EtOH hexamers but also shrinks to fit the smaller hydrogen-bonded MeOH hexamers. After adsorption of MeCN, the trigonal MAF-2 undergoes a drastic structural transformation to the triclinic phase. Novel hydrogen-bonded alcohol or nitrile hexamers are present in the guest-loaded crystal structures. Also remarkable, the cooperative flexibility of the $[Cu(tz)]_\infty$ scaffold and ethyl groups allows the diffusion of benzene with a large and anisotropic cross section, accompanied with a drastic structural transformation to the cubic phase. In contrast, the larger molecule cyclohexane is excluded from MAF-2, resulting in a very high benzene/cyclohexane selectivity.

In summary, by taking advantage of the kinetically controlled flexibility and multimode structural transformation ability, the cuprous triazolate reported here serves as a "smart" material, which possesses not only temperature-controllable sorption behavior but also superior separation performances and a multipurpose sensing ability.

Acknowledgment. This work was supported by the "973 Program" (2007CB815302), NSFC (No. 20531070), and NSF of Guangdong (No. 04205405).

Supporting Information Available: Crystallographic data in CIF format, PXRD patterns, TG and additional structural plots in PDF format. This material is available free of charge via the Internet at http://pubs.acs.org.

JA800550A